JOC*Article*

The Loss of Carbon Dioxide from Activated Perbenzoate Anions in the Gas Phase: Unimolecular Rearrangement via Epoxidation of the Benzene Ring

David G. Harman, Aravind Ramachandran, Michelle Gracanin,† and Stephen J. Blanksby*

Department of Chemistry, University of Wollongong, Wollongong NSW, 2522, Australia

blanksby@uow.edu.au

Received April 5, 2006

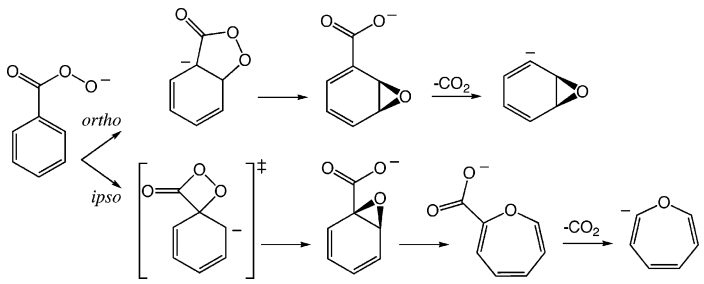

The unimolecular reactivities of a range of perbenzoate anions ($X-C_6H_5CO_3^-$), including the perbenzoate anion itself (X = H), nitroperbenzoates (X = *para*-, *meta*-, *ortho*-NO_2), and methoxyperbenzoates (X = *para*-, *meta*-OCH_3) were investigated in the gas phase by electrospray ionization tandem mass spectrometry. The collision-induced dissociation mass spectra of these compounds reveal product ions consistent with a major loss of carbon dioxide requiring unimolecular rearrangement of the perbenzoate anion prior to fragmentation. Isotopic labeling of the perbenzoate anion supports rearrangement via an initial nucleophilic aromatic substitution at the *ortho* carbon of the benzene ring, while data from substituted perbenzoates indicate that nucleophilic attack at the *ipso* carbon can be induced in the presence of electron-withdrawing moieties at the *ortho* and *para* positions. Electronic structure calculations carried out at the B3LYP/6-311++G(d,p) level of theory reveal two competing reaction pathways for decarboxylation of perbenzoate anions via initial nucleophilic substitution at the *ortho* and *ipso* positions, respectively. Somewhat surprisingly, however, the computational data indicate that the reaction proceeds in both instances via epoxidation of the benzene ring with decarboxylation resulting—at least initially—in the formation of oxepin or benzene oxide anions rather than the energetically favored phenoxide anion. As such, this novel rearrangement of perbenzoate anions provides an intriguing new pathway for epoxidation of the usually inert benzene ring.

Introduction

Peroxy acids, $RC(O)O_2H$, are used extensively in organic chemistry as reagents for synthesis.[1,2] Transformations, such as the Baeyer−Villiger oxidation of ketones,[3] epoxidation of olefins,[4] and the oxidation of nitrogen, sulfur, and phosphorus compounds,[5,6] are routinely achieved using peroxy acids. Base-promoted oxidations by peroxy acids have also been reported, including the oxidation of sulfoxides to sulfones[7,8] and the epoxidation of electron-deficient olefins.[9] Under basic conditions, the latter reaction has been rationalized as a two-step

* To whom correspondence should be addressed. Ph: ++61 2 4221 5484. Fax: ++61 2 4221 4287.
† Current address: Heart Research Institute, 145-147 Missenden Road, Camperdown, New South Wales, 2050, Australia.

(1) *Organic Peroxides*; Ando, W., Ed.; John Wiley: Chichester, UK, 1992.
(2) *Organic Peroxides*; Swern, D., Ed.; Wiley-Interscience: New York, 1972.
(3) Krow, G. R. In *Comprehensive Organic Synthesis*; Trost, B. M., Ed.; Pergamon Press: New York, 1991; Vol. 7, p 671.
(4) Rao, A. S. In *Comprehensive Organic Synthesis*; Trost, B. M., Ed.; Pergamon Press: New York, 1991; Vol. 7, p 357.
(5) Gilchrist, T. L. In *Comprehensive Organic Synthesis*; Trost, B. M., Ed.; Pergamon Press: New York, 1991; Vol. 7, p 735.
(6) Uemura, S. In *Comprehensive Organic Synthesis*; Trost, B. M., Ed.; Pergamon Press: New York, 1991; Vol. 7, p 757.
(7) Curci, R.; Modena, G. *Tetrahedron* **1966**, *22*, 1227.
(8) Curci, R.; Giovine, A.; Modena, G. *Tetrahedron* **1966**, *22*, 1235.

10.1021/jo060730a CCC: $33.50
Published on Web 09/22/2006

SCHEME 1

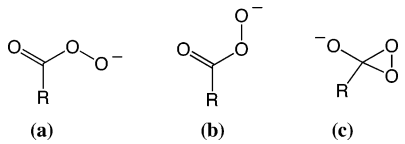

mechanism initiated by nucleophilic attack of the percarboxylate anion, $RC(O)O_2^-$, on the olefin.[9,10] Recent calculations by Washington and Houk,[11] however, suggest that stepwise addition of oxygen to the alkene occurs only in the presence of extremely electron-deficient (e.g., NO_2- and CN-substituted) alkenes, and the reaction generally proceeds via a concerted mechanism. Indeed, the concerted oxygen transfer by the percarboxylate anion has been exploited in organic synthesis to increase stereoselectivity[12,13] and regioselectivity[14] in the epoxidation of some olefins as well as in the preparation of acid-sensitive epoxides.[15,16] Peroxy acids have pK_a values[17] of ca. 8.3, and thus their conjugate bases—percarboxylate anions—are readily formed under alkaline conditions. Despite their importance in synthetic chemistry, there is limited understanding of the structure and reactivity of percarboxylate anions. Computational studies have shown that *anti* and *syn* conformations (Scheme 1a and b, respectively) exist as minima on the potential energy surface with the *syn* conformation generally preferred for the solvated anions by between 1 and 25 kJ mol^{-1} (depending on R).[11] Porter and co-workers have also proposed an isomeric oxydioxirane structure (Scheme 1c) which calculation suggests is only 5−50 kJ mol^{-1} (depending on the nature of R) more energetic than the percarboxylate anion.[18] Interconversion between the two isomers is predicted to occur over a relatively low barrier, and as such, the oxydioxirane anion may play a role in the observed oxygen scrambling in percarboxylate anions. Recent calculations, however, suggest that the oxydioxirane anion does not participate directly in the base-promoted epoxidation of alkenes by peroxy acids.[11]

In the present study, we have generated and detected a range of perbenzoate anions in the gas phase by electrospray ionization mass spectrometry (ESI-MS) of solutions of peroxybenzoic acids. Activation of these ions by collision with argon gas results in fragmentation and provides insight into the fundamental unimolecular reactivity of perbenzoate anions in the absence of solvent effects or counterions. While the unimolecular fragmentation of deprotonated alkyl peroxides has previously been reported,[19−21] the data presented here suggest that the unimolecular reactivity of percarboxylate anions is unique. In particular, we focus on a novel rearrangement of the perbenzoate anions that precedes fragmentation and results in loss of carbon dioxide. The mechanism for this rearrangement is elucidated via isotopic labeling studies, comparison of substituted homologues, and quantum chemical calculations.

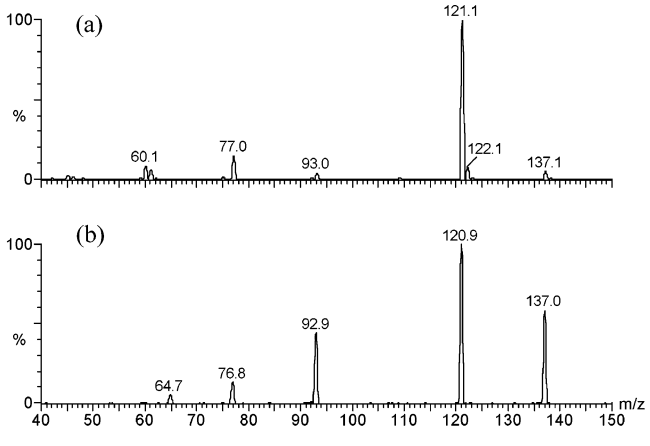

FIGURE 1. (a) The ESI-MS spectrum of a 10 μM aqueous methanol solution of $C_6H_5CO_3H$. (b) The ESI-MS/MS spectrum of the $C_6H_5CO_3^-$ anion, *m*/*z* 137. Both spectra were obtained using a QuattroMicro (Waters, Manchester) triple quadrupole mass spectrometer.

Results and Discussion

Electrospray Ionization of Peracids: The ESI-MS spectrum of an aqueous methanol solution of perbenzoic acid is given in Figure 1a and is representative of the spectra obtained from the other peracids examined in this study. It is significant that the peak at *m*/*z* 137 that corresponds to the perbenzoate anion, $C_6H_5CO_3^-$, is relatively weak compared to the intense signal for the benzoate anion, $C_6H_5CO_2^-$, at *m*/*z* 121. This difference in ion abundance may be due to the preferential ionization of benzoic acid present in the sample. Preferential deprotonation of benzoic acid would be anticipated based on its greater acid strength in both solution (i.e., p$K_a[C_6H_5CO_2H]$ = 4.2 compared to p$K_a[C_6H_5CO_3H]$ = 8.3)[17] and the gas phase (cf., $\Delta_{acid}H_{298}[C_6H_5CO_2H]$ = 1423 ± 12 kJ mol^{-1} compared to the only peracid measured, $\Delta_{acid}H_{298}[HCO_3H]$ = 1551 ± 9 kJ mol^{-1}).[22,23] Adding authentic benzoic acid to the electrospray solution increases the relative abundance of the *m*/*z* 121 ion; however, it fails to quench the perbenzoate signal at *m*/*z* 137, even in 1:1 mixtures of the two acids, as would be expected if ionization of the former were actively suppressing the latter. Alternatively, some perbenzoic acid molecules may undergo one-electron reduction during the electrospray process to form benzoate anions and hydroxyl radicals. This second possibility seems more likely as the oxidative dissociation of the O−O bond to form the benzoate anion and hydroxyl radical is thermodynamically favorable (electronic structure calculations give $\Delta H_{rxn} \sim -190$ kJ mol^{-1}), and indeed a decrease in the

(9) Zimmerman, H. E.; Singer, L.; Thyagarajan, B. S. *J. Am. Chem. Soc.* **1959**, *81*, 108.
(10) Apeloig, Y.; Karni, M.; Rappoport, Z. *J. Am. Chem. Soc.* **1983**, *105*, 2784.
(11) Washington, I.; Houk, K. N. *Org. Lett.* **2002**, *4*, 2661.
(12) Ye, D. Y.; Fringuelli, F.; Piermatti, O.; Pizzo, F. *J. Org. Chem.* **1997**, *62*, 3748.
(13) Fioroni, G.; Fringuelli, F.; Pizzo, F.; Vaccaro, L. *Green Chem.* **2003**, *5*, 425.
(14) Fringuelli, F.; Germani, R.; Pizzo, F.; Santinelli, F.; Savelli, G. *J. Org. Chem.* **1992**, *57*, 1198.
(15) Fringuelli, F.; Pizzo, F.; Germani, R.; Savelli, G. *Org. Prep. Proc. Int.* **1989**, *21*, 757.
(16) Fringuelli, F.; Germani, R.; Pizzo, F.; Savelli, G. *Tetrahedron Lett.* **1989**, *30*, 1427.
(17) Ripin, D.; Evans, D. pK_a Data, December 22, 2005, http://daecr1.harvard.edu/pKa/pka.html.
(18) Porter, N. A.; Yin, H. Y.; Pratt, D. A. *J. Am. Chem. Soc.* **2000**, *122*, 11272.
(19) Blanksby, S. J.; Bierbaum, V. M.; Ellison, G. B.; Kato, S. *Aust. J. Chem.* **2003**, *56*, 459.
(20) Schalley, C. A.; Schroeder, D.; Schwarz, H.; Moebus, K.; Boche, G. *Chem. Ber. Recueil* **1997**, *130*, 1085.
(21) Domingues, P.; Simoes, M. M. Q.; Cardoso, A. M.; Cavaleiro, A. M. V.; Cavaleiro, J. A. S.; Johnstone, R. A. W.; Ferrer-Correia, A. J. *Rapid Commun. Mass Spectrom.* **1999**, *13*, 93.
(22) Caldwell, G.; Renneboog, R.; Kebarle, P. *Can. J. Chem.* **1989**, *67*, 661.
(23) Bowie, J. H.; DePuy, C. H.; Sullivan, S. A.; Bierbaum, V. M. *Can. J. Chem.* **1986**, *64*, 1046.

SCHEME 2

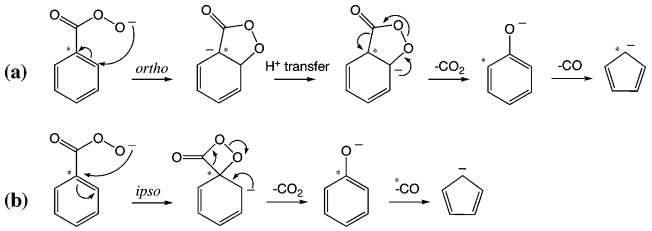

abundance of *m*/*z* 137 with respect to *m*/*z* 121 is observed with increasing electrospray voltage. Electrochemical processes of this kind have previously been observed at the electrospray capillary.[24] In either case, the result is a poor yield of the target perbenzoate anion, suggesting that negative ion electrospray ionization is a poor methodology for detection of small quantities of perbenzoic acids in an analytical context. The ion abundances achieved were, however, sufficient to examine the collision-induced fragmentation of the anions in the triple quadrupole mass spectrometer.

Collision-Induced Dissociation of $C_6H_5CO_3^-$: The ESI-MS/MS spectrum of the perbenzoate anion at *m*/*z* 137 is shown in Figure 1b. The base peak in this spectrum appears at *m*/*z* 121 and corresponds to a loss of atomic oxygen (16 Da) and formation of the benzoate anion from homolytic cleavage of the O−O bond. The bond dissociation energy required for this cleavage is calculated to be 84 kJ mol^{-1}. Surprisingly, however, an abundant fragment at *m*/*z* 93 is also observed that corresponds to a loss of 44 Da. This fragmentation may be rationalized in terms of the loss of carbon dioxide and formation of the phenoxide anion: a pathway likely to be highly exothermic. Furthermore, the fragment ion observed at *m*/*z* 65 in Figure 1b is consistent with secondary fragmentation of phenoxide via loss of carbon monoxide to form the aromatic cyclopentadienide anion (Scheme 2). The latter fragmentation has previously been reported for the collision-induced dissociation (CID) of the phenoxide anion.[25−27] The fragment ion at *m*/*z* 77 in Figure 1b is most likely the phenyl anion resulting from the loss of 60 Da from the precursor. This neutral loss corresponds to a concerted loss of CO_3 or, alternatively, may arise from decarboxylation of the benzoate anion (*m*/*z* 121) in a stepwise process. The former process seems unlikely on thermochemical grounds given the relative instability of neutral CO_3,[28] while the observation of facile decarboxylation of the benzoate anion in a separate CID experiment (Table 1) supports the stepwise mechanism.

The carbon dioxide loss is competitive with fragmentation via simple homolytic cleavage of the O−O bond and necessitates an efficient rearrangement of the percarboxylate moiety. Such a process has not previously been reported for peroxide anions but, in some respects, is analogous to the expulsion of carbon monoxide from deprotonated benzyl benzoates reported by Bowie and co-workers.[29] These authors proposed two possible mechanisms to account for the observed rearrangement, namely, a nucleophilic aromatic substitution at the *ipso* carbon (similar to the Smiles rearrangement)[26,30] or attack at the *ortho* position followed by proton transfer. In the context of the perbenzoate anion, these two mechanistic possibilities are outlined in Scheme 2.

TABLE 1. The Tandem Mass Spectra of Additional Precursor Ions Examined in This Study (i.e., those not given as figures; all spectra reported in this table were recorded on a triple quadrupole mass spectrometer except where indicated)

precursor ion	product ions *m*/*z* (% abundance)[a]
$[C_6H_5CO_2H - H]^-$	121(100), 77(59), 17(2)
[*cyclo*-$C_6H_{11}CO_3H - H]^-$	143(47), 127(56), 126(2), 125(26), 99(5), 97(100),[c] 95(41), 71(3), 69(12), 55(2), 45(12), 17(5)
$[C_6H_5{}^{13}CO_3H - H]^-$	138(16), 122(100), 93(23), 77(7), 65(6)
[^{13}C-1-ring-$C_6H_5CO_3H - H]^-$	138(8.0), 122(100), 94(15), 78(7), 66(4)
[^{13}C-1-ring-$C_6H_5CO_3H - H]^- \rightarrow$ ^{13}C-$C_6H_5O^-$	94(37), 66(100)[b]

[a] Ion abundance is given relative to the base peak. [b] This MS^3 spectrum was recorded on a ThermoFinnigan LTQ linear quadrupole ion trap. [c] The base peak at *m*/*z* 97 is likely to be deprotonated cyclohexanone, formed via stepwise and/or concerted loss of water and carbon monoxide.

Nucleophilic attack at the *ortho* position (Scheme 2a) should result in a less strained five-centered cyclic intermediate; however, the subsequent decarboxylation of this intermediate requires a 1,2-proton transfer which is likely to represent the rate-determining step. In contrast, the *ipso* mechanism does not require an energetic proton transfer but occurs via the more strained four-membered ring intermediate. These two possible rearrangement mechanisms were investigated using isotopic labeling and the examination of saturated homologues. The first step of both mechanistic proposals involves intramolecular nucleophilic attack on the aromatic ring. As such, the role of the benzene ring was examined by obtaining the ESI-MS/MS spectrum of the analogous saturated cyclic hydroperoxide, the $[M-H]^-$ anion from cyclohexylpercarboxylic acid (Table 1). This spectrum shows only a vanishingly small ion abundance corresponding to the loss of carbon dioxide, suggesting that indeed the aromatic ring plays a central role in the decarboxylation of perbenzoate anions. The ESI-MS/MS spectrum of the ^{13}C-isotopologue of perbenzoic acid labeled at the percarboxylate moiety (Table 1) shows exclusive formation of *m*/*z* 93, confirming that the percarboxylate carbon is lost as carbon dioxide. This observation is consistent with both the *ipso* and *ortho* mechanisms shown in Scheme 2. The ^{13}C-isotopologue of perbenzoic acid with the label at the 1-position in the benzene ring was also prepared. The ESI-MS/MS spectrum of the ring labeled isotopologue (Table 1) shows the loss of unlabeled carbon dioxide and formation of the ^{13}C-phenoxide fragment ion at *m*/*z* 94. This spectrum also shows that the cyclopentadienide fragment ion at *m*/*z* 66 carries the ^{13}C-label, indicating that the ^{13}C-labeled phenoxide anion has lost unlabeled carbon monoxide. Previous CID studies of labeled phenoxide indicate that the carbon bound to the oxygen is lost as carbon monoxide.[25−27] The asterisks in Scheme 2 indicate where the ^{13}C-label would be expected following loss of carbon dioxide via either the *ortho* or *ipso* pathway and thus where the label would be expected in the resulting phenoxide. Clearly, the *ipso*

(24) de la Mora, J. F.; Van Berkel, G. J.; Enke, C. G.; Cole, R. B.; Martinez-Sanchez, M.; Fenn, J. B. *J. Mass Spectrom.* **2000**, *35*, 939.
(25) Bowie, J. H.; Stringer, M. B. *Org. Mass Spectrom.* **1985**, *20*, 138.
(26) Eichinger, P. C. H.; Bowie, J. H.; Hayes, R. N. *J. Am. Chem. Soc.* **1989**, *111*, 4224.
(27) Binkley, R. W.; Tevesz, M. J. S.; Winnik, W. *J. Org. Chem.* **1992**, *57*, 5507.
(28) Pople, J. A.; Seeger, U.; Seeger, R.; Schleyer, P. v. R. *J. Comput. Chem.* **1980**, *1*, 199.
(29) Chia, C. S. B.; Taylor, M. S.; Dua, S.; Blanksby, S. J.; Bowie, J. H. *J. Chem. Soc., Perkin Trans. 2* **1998**, 1435.
(30) Warren, L. A.; Smiles, S. *J. Chem. Soc.* **1930**, 956.

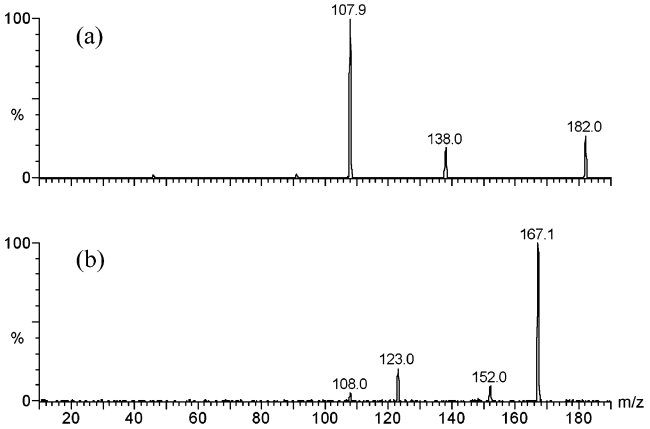

FIGURE 2. ESI-MS/MS spectra of a 10 μM aqueous methanol solution of (a) *para*-$NO_2-C_6H_4CO_3^-$ and (b) *para*-$CH_3O-C_6H_4CO_3^-$. Both spectra were obtained using a QuattroMicro (Waters, Manchester) triple quadrupole mass spectrometer.

mechanism (Scheme 2b) would result in unlabeled $C_5H_5^-$ at *m*/*z* 65, while the *ortho* mechanism (Scheme 2a) should produce a ^{13}C-labeled anion at *m*/*z* 66 as observed experimentally. To confirm that *m*/*z* 66 is a secondary fragment arising from decomposition of the labeled phenoxide, the CID of *m*/*z* 94 was conducted in an MS^3 experiment using an ion-trap mass spectrometer (Table 1). This experiment showed exclusive loss of unlabeled carbon monoxide, confirming that the rearrangement of the perbenzoate anion occurs via the *ortho* mechanism (Scheme 2a). This suggests that the proton transfer (rate-determining) step in the *ortho* rearrangement requires less activation energy than the four-centered intermediate in the *ipso* rearrangement. This raises the intriguing question of whether the activation energies and thus the reaction pathway are altered by substitution of the aromatic ring.

Collision-Induced Dissociation of $X-C_6H_4CO_3^-$: Nucleophilic aromatic substitution reactions are generally favored in aromatic compounds bearing electron-withdrawing groups due to stabilization of negative charge in the Meisenheimer intermediate[31,32] and the consequent lowering of the activation barrier. To further examine the generality and the mechanisms of perbenzoate decarboxylation, we synthesized substituted analogues and prepared the gas phase anions by ESI.

The CID spectrum of the $[M-H]^-$ anion from *para*-nitroperbenzoic acid (*m*/*z* 182) is shown in Figure 2a and reveals a significant abundance of the fragment ion at *m*/*z* 138 corresponding to loss of carbon dioxide and a base peak at *m*/*z* 108 that corresponds to the loss of CO_2 and NO. Interestingly, the loss of atomic oxygen by fission of the O−O bond—the base peak in the analogous spectrum of the perbenzoate anion (Figure 1b)—is not observed in the spectrum of the *para*-nitro-substituted homologue. Given that the O−O bond energy is expected to be largely unperturbed by substitution of the aromatic ring, this observation suggests that the activation energy required for carbon dioxide expulsion has been significantly reduced by nitro substitution. Surprisingly, however, enhancement of the rearrangement channel by substitution of a strong electron-withdrawing moiety at the *para* position is indicative of nucleophilic attack at the *ipso* rather than the *ortho*

SCHEME 3

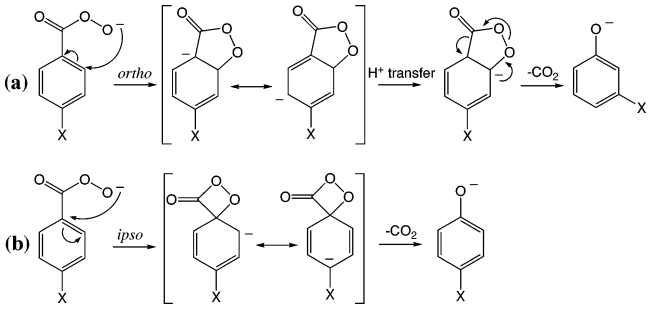

position, as illustrated by the resonance structures in Scheme 3 and in apparent contradiction of labeling data from the perbenzoate anion. This possibility was further investigated by comparison of the CID spectrum of *m*/*z* 138 ions formed by loss of CO_2 in the ion source of the mass spectrometer with the isobaric $[M-H]^-$ ions from *ortho*-, *meta*-, and *para*-nitrophenol: the putative products of the decarboxylation. These data are presented in Table 2 and show that fragmentation of the source-formed $[M-H-CO_2]^-$ ion from *para*-nitroperbenzoic acid occurs predominantly via loss of NO and NO_2 and formation of the NO_2 anion, which are analogous to the fragments and relative abundances observed from the $[M-H]^-$ anion of *para*-nitrophenol at the same collision energy. In contrast, the relative abundances of these losses are different for the *meta*- and *ortho*-nitrophenoxide anions (Table 2), and furthermore, these species show significant fragment ions at *m*/*z* 91 and 80 not observed for the *para*-regioisomer. These data suggest that the structure of the $[M-H-CO_2]^-$ ion from *para*-nitroperbenzoic acid is most closely related to the *para*-nitrophenoxide anion and is thus consistent with loss of carbon dioxide from the perbenzoate anion occurring via the *ipso* mechanism (Scheme 3b).

A similar trend was observed for *ortho*-nitroperbenzoic acid, which also showed significant loss of carbon dioxide and a product ion with strong structural similarities to *ortho*-nitrophenoxide (Table 2). In contrast, the *meta*-nitroperbenzoate anion demonstrated less fragmentation with a normalized precursor ion abundance of 40% compared to 28 and 17% for *ortho*- and *para*-regioisomers, respectively. Furthermore, the CID spectrum of source-formed $[M-H-CO_2]^-$ product ions (Table 2) did not match any of the isomeric nitrophenoxide anions and indeed revealed abundant fragment ions not observed for any of the authentic phenoxides, such as *m*/*z* 73, 63, and 41. These data indicate that the *meta*-isomer undergoes loss of carbon dioxide via a mechanism different than that of the *ortho*- and *para*-isomers. The alternative mechanism does not appear to result in direct formation of pure nitrophenoxide anions as predicted by Scheme 3, and thus an alternative explanation is required.

For comparison, the effects of substitution with an electron-donating group were also investigated, and the CID spectra of *meta*- and *para*-methoxyperbenzoate anions are presented in Table 3. Measured at the same collision energy as the nitro-substituted homologues, the methoxyperbenzoate anions showed significantly less fragmentation corresponding to the loss of carbon dioxide and less fragmentation overall with normalized precursor ion abundances of around 70% compared to 20−40% for the nitroperbenzoates. These observations are consistent with the destabilization of intermediates in the aromatic substitution reaction by the electron-donating methoxy moiety. The CID

(31) Meisenheimer, J. *Liebigs Ann. Chem.* **1902**, *323*, 205.
(32) Artamkina, G. A.; Egorov, M. P.; Beletskaya, I. P. *Chem. Rev.* **1982**, *82*, 427.

TABLE 2. (a) The Tandem Mass Spectra of the $[M-H]^-$ Ions from Nitroperbenzoic Acids (collision energy = 10 eV) and (b) The Tandem Mass Spectra of Source-Formed $[M-H-CO_2]^-$ Ions from Nitroperbenzoic Acids and the $[M-H]^-$ Ions Formed from Related Phenols (collision energy = 20 eV)[a]

(a) tandem mass spectra of the $[M-H]^-$ ions

m/z	182	152	138	136	135	120	108	92	91	80	64	46
loss or fragment	[M−H]	−NO	$-CO_2$	$-NO_2$	$-HNO_2$	$-NO_2$ −O	$-CO_2$ −NO	$-CO_2$ $-NO_2$	$-CO_2$ $-HNO_2$	C_5H_4O	C_5H_4	NO_2
ortho-NO_2	72[b](28)[c]	9(4)	100(39)	4(2)		1(1)	44(17)	14(5)	2(1)	2(1)	1(0)	7(3)
meta-NO_2	96(40)	2(1)	36(15)				6(3)		100(41)			2(1)
para-NO_2	24(17)		17(12)				100(69)		2(1)			2(1)

(b) tandem mass spectra of source-formed $[M-H-CO_2]^-$ ions

m/z	138	108	94	92	91	80	73	63	46	41
loss or fragment		−NO	$-CO_2$	$-NO_2$	$-HNO_2$	C_5H_4O	$C_2H_3NO_2$	C_5H_3	NO_2	C_2HO
ortho-NO_2 peracid	58	100	7	21	7	16			62	
meta-NO_2 peracid	43	100		13	70	19	14	28	68	38
para-NO_2 peracid	44	100		14	2	2			18	
ortho-NO_2 phenol	59	100		28	13	8			78	
meta-NO_2 phenol	37	49		4	7	67			100	

[a] Ion abundances are reported for each *m/z* as a percentage of the base peak, and for some spectra, normalized ion abundances are provided in parentheses. All spectra reported in these tables were recorded on a Waters QuattroMicro triple quadrupole mass spectrometer. [b] Ion abundance as a percentage of the base peak. [c] Normalized ion abundance as a percentage of total ion abundance calculated from $I_n/\sum I_i \times 100$.

TABLE 3. (a) The Tandem Mass Spectra of the $[M-H]^-$ Ions from Methoxyperbenzoic Acids (collision energy = 10 eV) and (b) the Tandem Mass Spectra of Source-Formed $[M-H-CO_2]^-$ Ions from Methoxyperbenzoic Acids and the $[M-H]^-$ Ions Formed from Related Phenols (collision energy = 10 eV)[a]

(a) tandem mass spectra of the $[M-H]^-$ ions

m/z	167	152	123	108
loss or fragment	[M−H]	$-CH_3$	$-CO_2$	$-CH_3$ $-CO_2$
meta-OCH_3	100[b](68)[c]	26(18)	5(3)	15(11)
para- OCH_3	100(73)	10(7)	22(16)	5(4)

(b) tandem mass spectra of source-formed $[M-H-CO_2]^-$ ions

m/z	123	108	105	95	93	91	80	79	77	61
loss or fragment	[M−H]	$-CH_3$	$-H_2O$	−CO	$-CH_2O$	$-CH_3O$ −H	$-CH_3$ −CO	$-CO_2$	C_6H_5	C_6H
meta-OCH_3 peracid	100	60		18		4	3	3	9	
para-OCH_3 peracid	100	38	4	14	3				2	5
ortho-OCH_3 phenol	56	100		2						
meta-OCH_3 phenol	100	53		1						
para-OCH_3 phenol	17	100		1						

[a] Ion abundances are reported for each *m/z* as a percentage of the base peak, and for some spectra, normalized ion abundances are provided in parentheses. All spectra reported in these tables were recorded on a Waters QuattroMicro triple quadrupole mass spectrometer. [b] Ion abundance as a percentage of the base peak. [c] Normalized ion abundance as a percentage of total ion abundance calculated from $I_n/\sum I_i \times 100$.

spectra obtained from source-formed $[M-H-CO_2]^-$ ions from both *meta*- and *para*-methoxyperbenzoic acid are presented in Table 3 and are similar in fragment ions and abundances to each other as well as to the *meta*-methoxyphenoxide anion. This is consistent with minimization of the destabilizing effects of the electron-donating substituent in the *ortho* mechanism for *para*-methoxyperbenzoate (Scheme 3a) and in the *ipso* mechanism in the case of *meta*-methoxyperbenzoate (Scheme 3b). Some variation was observed between the $[M-H-CO_2]^-$ ions from the methoxyperbenzoic acids and the authentic methoxyphenoxides, most notably in the relative abundance of ions at *m/z* 95 corresponding to carbon monoxide loss. As was the case for the *meta*-nitroperbenzoate anions, this indicates the presence of isomeric product ions and thus alternative or competing mechanisms for CO_2 loss from the perbenzoate.

These data indicate that *both* rearrangement mechanisms originally proposed in Scheme 2 are plausible and that the energetic requirements are comparable and are influenced by the nature and position of substituents on the benzene ring. Furthermore, there is evidence that the loss of CO_2 does not result solely in pure phenoxide ions as suggested by Schemes 2 and 3 but that isomeric ions are also present.

TABLE 4. The Electronic Energy (Hartrees), Zero-Point (Hartrees) and Relative Energies (0 K, kJ mol^{-1}) Calculated at the B3LYP/6-311++G(d,p) for All Stationary Points Involved in the Rearrangement of the Perbenzoate Anion as Illustrated in Figure 3[a]

molecular anion	electronic energy	zero-point correction	relative energy
$C_6H_5-CO_3^-$	−495.52139	0.10407	0
ipso-**TS1** (−568 cm^{-1})	−495.48059	0.10135	100.0
ipso-**IM1**	−495.57069	0.10438	−128.6
ipso-**TS2** (−413 cm^{-1})	−495.56461	0.10308	−116.1
ipso-**IM2**	−495.57369	0.10388	−137.8
ipso-**P1**	−306.85362	0.08712	
ortho-**TS1** (−323 cm^{-1})	−495.49161	0.10317	75.9
ortho-**IM1**	−495.49680	0.10394	64.2
ortho-**TS2** (−503 cm^{-1})	−495.48366	0.10239	94.7
ortho-**IM2**	−495.57260	0.10486	−132.4
ortho-**P2**	−306.84514	0.00944	
ortho-**TS3** (−474 cm^{-1})	−495.45073	0.10049	176.1
$C_6H_5O^-$	−306.99406	0.08945	
CO_2	−188.64691	0.01169	

[a] Transition state imaginary frequencies are provided in parentheses, and structures of all stationary points are provided as Supporting Information.

Electronic Structure Calculations. The experimental data discussed above suggest that carbon dioxide loss from perben-

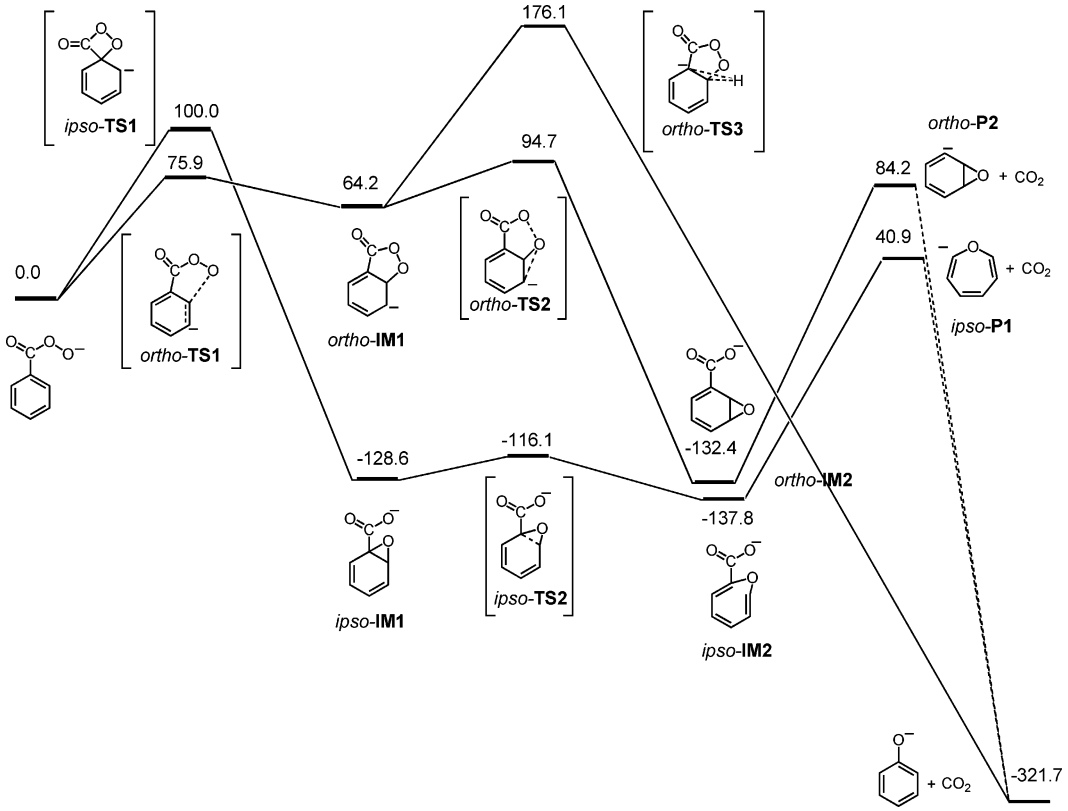

FIGURE 3. Reaction coordinate diagram for the unimolecular rearrangement of $C_6H_5CO_3^-$ calculated at the B3LYP/6-311++G(d,p) level of theory. All energies are given in kJ mol^{-1}.

zoate anions can proceed via either an *ipso* or an *ortho* mechanism (Scheme 2) depending on the nature and position of substitution of the aromatic ring. Electronic structure calculations have been performed to investigate these mechanisms in detail. The calculated potential energy surface for rearrangement of the $C_6H_5-CO_3^-$ anion and subsequent decarboxylation is shown in Figure 3 with energies given relative to the percarboxylate anion. The electronic energies of critical stationary points are listed in Table 2 with molecular structures and full Cartesian coordinates provided as Supporting Information.

The optimized structure of the *anti*-conformation of the perbenzoate anion is provided as Supporting Information, and energies of all stationary points are relative to this species. Although the *syn*-conformation (not shown) is 0.8 kJ mol^{-1} lower in energy at the chosen level of theory, only the *anti*-conformation is suitably oriented to undergo the nucleophilic aromatic substitution reactions investigated here. Considering the *ortho* mechanism first, attack of the peroxide oxygen at the *ortho* carbon occurs via the transition state *ortho*-**TS1**. This presents a barrier of 75.9 kJ mol^{-1} to rearrangement to the five-centered endoperoxide, *ortho*-**IM1**, which lies some 64.2 kJ mol^{-1} above the percarboxylate minimum. The structure of the endoperoxide is representative of a Meisenheimer intermediate with a near tetrahedral geometry about the *ortho* carbon with the adjacent C−C bonds lengthened from a benzene-like 1.40 Å in the perbenzoate anion to an alkane-like 1.50 Å in the intermediate structure. The endothermicity of this first step can be attributed to the loss of aromaticity which is somewhat offset by resonance stabilization of the negative charge over several carbon centers and the carbonyl oxygen. A transition state, *ortho*-**TS3**, was located for the 1,2-proton transfer step postulated in Scheme 2a. Intrinsic reaction coordinate calculations

SCHEME 4

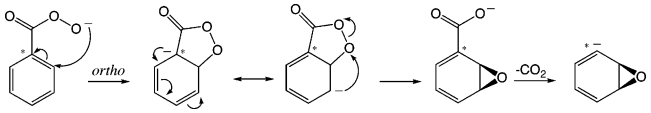

on this transition state show that it connects the endoperoxide intermediate, *ortho*-**IM1**, with the minimum corresponding to phenoxide anion and carbon dioxide. The structure for *ortho*-**TS3** shows a late transition state with the proton already bound at the *ipso* position, reminiscent of the intermediate structure proposed in Scheme 2a. The geometry of *ortho*-**TS3** reveals a lengthening of the O−O bond to 1.51 Å in preparation for cleavage of peroxide bond and coincident lengthening of the C−C(O)O bond to 1.51 Å for subsequent decarboxylation. Although the phenoxide product channel accessed by this transition state represents the global minimum—some 322 kJ mol^{-1} lower in energy than the perbenzoate precursor—the barrier to this process is significant, E_a = 176 kJ mol^{-1}. Interestingly, a lower energy pathway to decarboxylation was identified whereby the endoperoxide intermediate, *ortho*-**IM1**, rearranges via transition state, *ortho*-**TS2**, to form the intermediate epoxide *ortho*-**IM2**. This reaction is driven by the cleavage of the weak peroxide bond and formation of the stable carboxylate anion as outlined in Scheme 4. The barrier to this process is only 95 kJ mol^{-1}, and the rearrangement provides the isomerized intermediate with sufficient internal energy to undergo decarboxylation resulting in the product ion, *ortho*-**P2**. Although this product is more than 400 kJ mol^{-1} less stable than the isomeric phenoxide anion, the overall activation energy for this exit channel is some 81 kJ mol^{-1} lower than the phenoxide forming mechanism (see Figure 3).

SCHEME 5

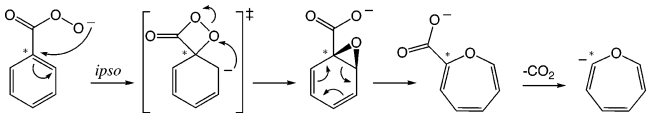

In contrast, rearrangement of the perbenzoate anion via nucleophilic aromatic substitution at the *ipso* carbon is calculated to occur via the transition state *ipso*-**TS1** that lies 100 kJ mol^{-1} above the entrance channel. The optimized structure of the bicyclic transition state is reminiscent of the reactive intermediate proposed in Scheme 2b. The additional strain of the four-membered ring in addition to the inability to delocalize the charge onto oxygen in this structure may account for the greater activation energy (24 kJ mol^{-1}) required for *ipso* rearrangement. No bicyclic minimum could be located, and intrinsic reaction coordinate calculations on *ipso*-**TS1** show that it is connected to the substituted benzene oxide intermediate *ipso*-**IM1** rather than the phenoxide exit channel predicted in Scheme 2b. The structure of *ipso*-**IM1** is similar in geometry and energy to the isomeric epoxide *ortho*-**IM2** discussed above. The benzene oxide-like intermediate, *ipso*-**IM1**, tautomerizes over a small barrier (E_a = 13 kJ mol^{-1}) to form the more stable substituted oxepin *ipso*-**IM2**. This pathway is analogous to the benzene oxide−oxepin tautomerism calculated by Kassaee et al., who found activation barriers of similar magnitude.[33] The reaction intermediate *ipso*-**IM2** formed by rearrangement of the perbenzoate anion has sufficient internal energy to undergo decarboxylation (E_a = 213 kJ mol^{-1}) to form the deprotonated oxepin anion, *ipso*-**P1**. No transition state could be located for this process, nor for direct decarboxylation of *ipso*-**IM1**. In both instances, minimization of the carboxylate anions starting from a range of C−C(O)O bond lengths resulted in either the starting geometry or *ipso*-**P1** and carbon dioxide: no stable minimum corresponding to the deprotonated benzene oxide tautomer could be located. Thus these calculations suggest a revision of the mechanism for *ipso* rearrangement as outlined in Scheme 5.

To summarize the computed pathways for decarboxylation of the perbenzoate anion, Figure 3 shows that the lowest energy pathway is via initial nucleophilic aromatic substitution at the *ortho* position as anticipated from experiment. Surprisingly, however, the lowest energy pathways for decarboxylation via either *ortho* or *ipso* mechanism do not result, at least initially, in the thermodynamically favored phenoxide anion but rather isobaric oxepin or benzene oxide anions. It seems highly probable that subsequent rearrangement of these ions will result in formation of the global minimum, but this may require additional activation and is beyond the scope of this study. The revised mechanisms shown in Schemes 4 and 5 appear consistent with the results of the ^{13}C-labeling studies discussed earlier. The position of the label in each of these schemes is indicated with an asterisk and shows that for the *ipso* mechanism (Scheme 5) the label ends up adjacent to the oxygen in the resulting oxepin anion, suggesting it would be lost in any subsequent decarbonylation reaction. Conversely, for the *ortho* mechanism (Scheme 4), the label is not bound to the oxygen and is thus unlikely to be lost as carbon monoxide and thus a ^{13}C-labeled cyclopentadienide anion would be expected in line with experimental observations.[34]

The effects of substitution on the rearrangement of the perbenzoate were also modeled by calculating the reaction coordinate data for the *para*-methoxyperbenzoate (Figure 4a) and *para*-nitroperbenzoate (Figure 4b). Full energy and geometric data for each of the stationary points in these figures are provided as Supporting Information. Considering the case of nitro substitution first, the activation barrier to nucleophilic aromatic substitution at the *ipso* position is lowered by 55 kJ mol^{-1} with respect to the unsubstituted system, while the activation energy for the rate-determining step along the *ortho* pathway remains largely unperturbed by the nitro moiety. This preferential stabilization by the electron-withdrawing nitro substituent on the *ipso*-**TS1** transition state may be understood in terms of the delocalization of electron density onto the *para*-carbon as outlined in Scheme 3b. Interestingly, the transition state for 1,2-proton-transfer-coupled decarboxylation, *ortho*-**TS3**, is also significantly lowered by the presence of the nitro moiety and becomes more favorable than the competing epoxidation channel. Despite the large decrease in activation energy (ca. 100 kJ mol^{-1}) for this phenoxide-forming pathway, all *ortho* mechanisms are well above the alternative *ipso* pathway that requires only 45 kJ mol^{-1} of activation energy. Conversely, the same rationale would predict an increase in the activation energy required for the *ipso* rearrangement in the presence of the electron-donating methoxy substituent. Indeed this trend is observed, with the computational data presented in Figure 4a showing the *ipso* pathway is destabilized by some 17 kJ mol^{-1} in the presence of the methoxy group, while the *ortho* coordinate is largely unaffected by the substitution. The computational data would thus predict a change in the mechanism leading to loss of carbon dioxide with the change from electron-donating to electron-withdrawing substituents at the *para* position. This result is thus consistent with the experimental findings outlined above. Furthermore, both potential energy surfaces reveal that decarboxylation by either mechanism results, at least initially, in a substituted oxepin or benzene oxide anions rather than phenoxide ions as originally hypothesized. While subsequent rearrangement to the global minimum seems likely, this may occur to a greater or lesser extent depending on the internal energy distribution of the nascent product ions. This may account for some of the differences observed experimentally between source-formed product ions and authentic phenoxide anions (Tables 2 and 3).

Conclusions

The isotopic labeling data from the perbenzoate anion provide strong evidence for unimolecular loss of carbon dioxide via the *ortho* mechanism proposed in Scheme 2a. The combination of substituent studies and electronic structure calculation, however, reveals a somewhat more complex reaction manifold with competing *ortho* and *ipso* mechanisms that have similar activation energies directly influenced by the nature and position of substituents on the aromatic ring. These data also indicate, rather surprisingly, that the loss of carbon dioxide does not lead directly to the phenoxide product ions but rather proceeds via initial epoxidation of the benzene ring forming benzene oxide

(33) Kassaee, M. Z.; Arshadi, S.; Ahmadi-Taheri, N. *J. Mol. Struct.* **2005**, *715*, 107.

(34) Hydrogen scrambling, which might confuse these experimental results, has not been observed for deuterium-labeled $C_6H_5O^-$ anions even under high energy collision conditions.[27]

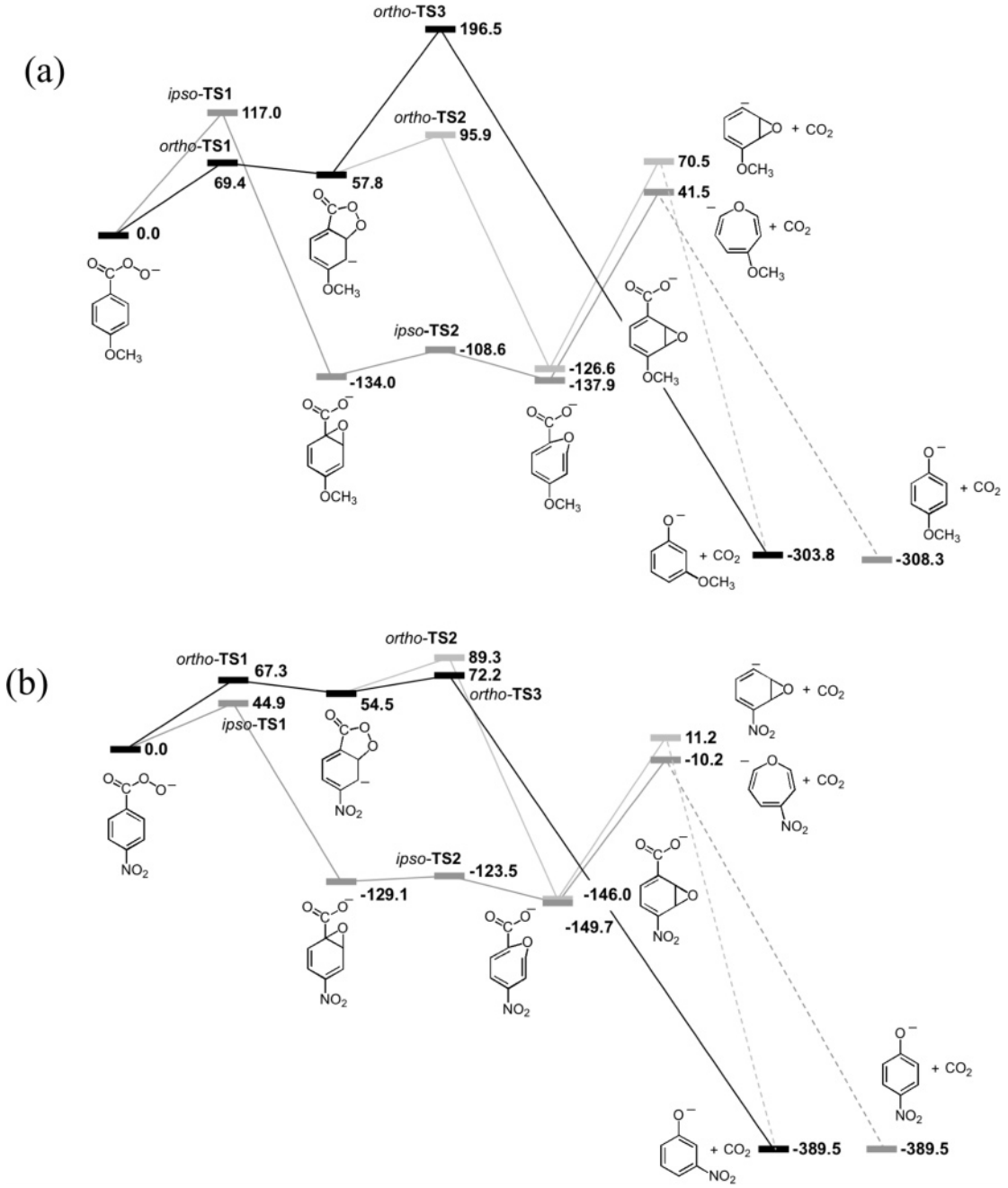

FIGURE 4. Reaction coordinate diagrams for the unimolecular rearrangement and decarboxylation of *para*-$XC_6H_5CO_3^-$, where (a) X = OCH_3 and (b) X = NO_2. All calculations were conducted at the B3LYP/6-311++G(d,p) level of theory with full geometric and energetic descriptions of stationary points available as Supporting Information. Energies are given relative to the perbenzoate precursor ions in units of kJ mol^{-1}. The dashed lines indicate the possibility for further rearrangement of oxepin and benzene oxide isomers to phenoxide following decarboxylation that is outside the scope of the present study.

or oxepin anions that may subsequently rearrange to the global minimum (Schemes 4 and 5).

Simple organic reactions that result in the oxidation of benzene are relatively few due to the aromatic stability of the benzene ring. This is one of the reasons that dioxin pollutants are so persistent in the environment and so much effort is currently being expended in developing enzymatic and metal-based catalysts to facilitate oxidative degradation of these aromatic compounds.[35] It is intriguing therefore that in this study we have observed facile unimolecular epoxidation of the benzene ring during fragmentation of perbenzoate anions. The decarboxylation reaction driving the epoxidation competes favorably with homolytic processes, such as the loss of atomic oxygen, nitric oxide, or methyl radicals. This *intramolecular* epoxidation of the aromatic ring is analogous to the solution phase *intermolecular* epoxidation of alkenes by percarboxylate anions discussed earlier.[11] It would therefore be of interest for future studies to investigate whether perbenzoate anions can initiate (i) analogous intramolecular aromatic epoxidation reactions in solution[36] and, conversely, (ii) intermolecular aromatic epoxidation reactions in the gas phase.

(35) Finocchio, E.; Busca, G.; Notaro, M. *Appl. Catal., A* **2006**, *62*, 12.

Experimental Section

Mass Spectrometry. Standard solutions of peracids (10 μM) were prepared in aqueous methanol (50% v/v) with the pH adjusted to 9−10 using aqueous ammonia. Mass spectra were obtained using a QuattroMicro triple quadrupole mass spectrometer (Waters, Manchester, UK). Spectra were obtained by infusion of the standard solution (10 μL/min), typical settings were cone voltage 60 V, capillary voltage 3 kV, source temperature 80 °C. ESI-MS spectra were obtained by scanning Q1 while operating Q3 in R_f-only mode. Resolution for ESI-MS and ESI-MS/MS experiments was typically 0.5 Th across the entire mass range. ESI-MS/MS spectra were obtained by mass-selecting the parent ion using Q1 and scanning for product ions using Q3. Argon was used as the collision gas at a pressure of 4×10^{-3} Torr. ESI-MS and ESI-MS/MS spectral data presented in this paper result from the average of at least 50 scans. The data were baseline subtracted (40% background subtract with a first-order polynomial) and smoothed (two mean smooths using a peak width of 0.5 Th) using the MassLynx software (Waters, Manchester UK). High-resolution ESI-MS spectra of deprotonated peracids were obtained using a Q-ToF Ultima quadrupole-time-of-flight instrument (Waters, Manchester, UK). MS^3 spectra were obtained in a LTQ quadrupole linear ion-trap mass spectrometer (ThermoFinnigan, San Jose, USA).

Synthesis and Characterization of Perbenzoic acids. Most peracids were prepared by procedures based on those of Swern and co-workers, in which a carboxylic acid was suspended in methanesulfonic acid and treated with concentrated aqueous hydrogen peroxide.[37,38] These preparations were carried out in open beakers behind a blast shield as a precaution. The highly reactive 4-methoxyperbenzoic acid was prepared from the acid chloride by adapting a procedure of Lefort and co-workers.[39] Peracids were stored in the dark at −18 °C, and purities were determined iodometrically by treatment of a weighed sample in acetone/acetic acid solution with excess saturated aqueous KI, then titration of the liberated iodine with a standard aqueous $Na_2S_2O_3$ solution.[40] FT-IR spectra were obtained in chloroform solution. Additional characterization is provided for previously reported compounds where literature data are absent. Yields are adjusted for purity.

CAUTION: Peracids may explode when heated or detonated by shock or sparks and are chemically incompatible with strong reducing agents, transition metals, and easily oxidized organic compounds. Open reaction vessels and nonflammable solvents were used wherever possible as recommended by Swern.[2] Excessive heat and agitation of peracid solutions was avoided during rotary evaporation, and samples were stored at −18 °C.

Concentration of Hydrogen Peroxide. A Dreschel bottle was charged with aqueous H_2O_2 (500 mL, 44% m/m), and dry air was bubbled slowly through the solution via a sintered glass frit at room temperature until the volume reduced to ~175 mL (6 weeks). The concentration was found to be 84% by titration against an acidified $KMnO_4$ standard solution. This sample was purified by evaporation and cold-trapping (liq. N_2) almost to dryness under high vacuum at room temperature. Concentration under vacuum at room temperature yielded a 92% solution.

CAUTION: Decomposition of hydrogen peroxide to oxygen and water can occur rapidly under high pH conditions and by exposure to transition metals and their ions. Contact with combustibles may result in a fire or explosion. Build-up of oxygen can also occur due to gradual decomposition of high purity H_2O_2, and thus storage containers must not be sealed.[41,42] The highly concentrated hydrogen peroxide prepared in this study was stored in the dark at 4 °C in a clean Schott bottle with a vented cap.

Cyclohexanepercarboxylic acid. Cyclohexanecarboxylic acid (14 mg, 0.11 mmol) was added to a stirred solution of H_2O_2 (92%, 0.30 g, 8.0 mmol) in methanesulfonic acid (MsOH, 0.55 g, 5.7 mmol) at 0 °C. The mixture was heated gradually to 40 °C and kept at that temperature for 2 h, before cooling to 0 °C and diluting with cold H_2O (5 mL). The resulting mixture was extracted with CH_2Cl_2 (5 mL), the extract was washed with H_2O (5 mL), dried ($MgSO_4$), and rotary evaporated at room temperature to yield a colorless oil (16 mg, 97% yield): δ_H ($CDCl_3$, 300 MHz) 1.20−1.38 (3H, m), 1.40−1.55 (2H, m), 1.64−1.71 (1H, m), 1.75−1.78 (2H, m), 1.87−1.95 (2H, m), 2.31−2.39 (1H, m), 11.39 (1H, br); δ_C ($CDCl_3$, 75 MHz) δ 25.3, 25.7, 28.8, 42.8, 161.6; *m*/*z* (ESI) found 143.0732, calcd for $C_7H_{11}O_3$ $(M - H)^-$ 143.0708.

Perbenzoic acid.[37] Hydrogen peroxide (3.2 g, 44% m/m, 41 mmol) was added dropwise to a stirred suspension of benzoic acid (3.7 g, 30 mmol) in MsOH (14.4 g, 150 mmol) at 40 °C. After 4.5 h, the colorless solution was cooled, treated with ice (10 g), followed by saturated aqueous $(NH_4)_2SO_4$ solution (10 mL). The resulting mixture was extracted with CH_2Cl_2 (3×10 mL), the combined extracts were washed with saturated aqueous $(NH_4)_2SO_4$ (3×10 mL), dried ($MgSO_4$), and concentrated by rotary evaporation at room temperature to afford a white crystalline solid (4.2 g, 83% yield) that was analyzed as 83.0% peracid by iodometric titration. A small amount of the crude perbenzoic acid was purified further by flash chromatography ($R_f = 0.3$, CH_2Cl_2 on silica) for characterization: ν_{max}/cm^{-1} 3514 br, 3265 br, 1728 vs, 935 w; δ_H ($CDCl_3$, 500 MHz) 7.50 (2H, dd, $J = 7.8$ Hz), 7.65 (1H, dd, $J = 7.8$, 0.98 Hz), 8.00 (2H, m, $J = \sim 8$, 0.98 Hz), 11.64 (1H, s); δ_C ($CDCl_3$, 125 MHz) 125.2, 128.9, 129.3, 134.4, 168.1; *m*/*z* (ESI) found 137.0270, calcd for $C_7H_5O_3$ $(M - H)^-$ 137.0239.

Perbenzoic acid-Ring-1-^{13}C and Perbenzoic acid-Carboxy-^{13}C. The ^{13}C-isotopologues of perbenzoic acid, perbenzoic acid-ring-1-^{13}C (34%), and perbenzoic acid-carboxy-^{13}C (33%) were prepared and purified similarly on a 0.4 mmol scale in the yields indicated, from benzoic acid-ring-1-^{13}C (Icon Isotopes, 99 atom %) and benzoic acid-carboxy-1-^{13}C (Sigma-Aldrich 99 atom %), respectively. The only differences were (a) the hydrogen peroxide addition was done at 0 °C and the reaction was immediately allowed to warm to room temperature; (b) the CH_2Cl_2 extracts were washed with cold water instead of aqueous $(NH_4)_2SO_4$.

2-Nitroperbenzoic acid.[37] To a stirred suspension of 2-nitrobenzoic acid (5.0 g, 30 mmol) in MsOH (14.4 g, 150 mmol) at 35 °C was added aqueous H_2O_2 (92% m/m, 3.6 g, 98 mmol) dropwise, at a rate which kept the temperature below 40 °C. After 4 h, the mixture was cooled to 10 °C and treated with ice (10 g) followed by ice water (20 mL). The resulting solid was filtered, washed twice with ice water, and dried in vacuo at room temperature to yield pale yellow crystals (4.5 g, yield 64%) that were analyzed as 79.0% peracid by iodometric titration. The crude peracid was suspended in water (30 mL) at 10 °C, and aqueous NaOH (10 mL, 0.2% w/v, 6 mmol) was added to extract the residual carboxylic acid. The suspension was filtered, and the precipitate was washed with ice water (20 mL) and dried in vacuo. Recrystallization from Et_2O/pentane (twice) yielded pale yellow crystals that were analyzed as 100% peracid: mp 95.5−96.5 °C (lit. 95−96 °C in a sealed capillary);[37] ν_{max}/cm^{-1} 3502 br, 3304 br, 1755 vs, 962 w; δ_H (CD_3OD (19 mol %) in $CDCl_3$, 500 MHz) 2.85 (1H, br), 7.69−7.79 (3H, m), 8.10 (1H, dd, $J = 8.0$, 1.0 Hz); δ_C ($CDCl_3$, 75 MHz) 124.4, 124.9, 129.8, 132.3, 133.8, 147.0, 165.7; *m*/*z* (ESI) found 182.0116, calcd for $C_7H_4NO_5$ $(M - H)^-$ 182.0089.

(36) Preliminary investigations in our laboratory find that both perbenzoic acid and 4-nitroperbenzoic acid undergo minimal reaction in aqueous alkaline solution even when heated at 120 °C in a sealed vessel for 3 days.

(37) Silbert, L. S.; Siegel, E.; Swern, D. *J. Org. Chem.* **1962**, *27*, 1336.
(38) Silbert, L. S.; Siegel, E.; Swern, D. *Org. Synth.* **1963**, *43*, 93.
(39) Nedelec, J. Y.; Sorba, J.; Lefort, D. *Synthesis* **1976**, *12*, 821.
(40) Swern, D. *Organic Reactions*; Wiley: New York, 1953; Vol. 7, p 378.
(41) Schumb, W. C.; Satterfield, C. N.; Wentworth, R. L. *Hydrogen Peroxide*; Reinhold Publishing: New York, 1955; p 152.
(42) Shanley, E. S. In *Organic Peroxides*; Swern, D., Ed.; Wiley-Interscience: New York, 1972; Vol. 3, p 341.

3-Nitroperbenzoic acid.[43] Procedure as for 2-nitroperbenzoic acid. 3-Nitrobenzoic acid (5.0 g, 30 mmol), MsOH (14.4 g, 150 mmol), and H_2O_2 (3.6 g of 88%, 93 mmol) afforded the product as pale yellow crystals (4.9 g, 89%), which was analyzed as 99.7% peracid by iodometric titration: mp 80−82 °C; ν_{max}/cm^{-1} 3508 br, 3286 br, 1743 vs, 922; δ_H ($CDCl_3$, 300 MHz) 7.77 (1H, t, J = 8.1 Hz), 8.34 (1H, ddd, J = 7.6, 1.8, 1.2 Hz), 8.52 (1H, ddd, J = 8.1, 2.3, 1.2 Hz), 8.85 (1H, m), 11.55 (1H, br); δ_C ($CDCl_3$, 75 MHz) 124.4, 127.1, 128.7, 130.3, 134.8, 148.3, 165.8; *m*/*z* (ESI) found 182.0128, calcd for $C_7H_4NO_5$ $(M - H)^-$ 182.0089.

4-Nitroperbenzoic acid.[37,43] Preparation as for 2-nitroperbenzoic acid. 4-Nitrobenzoic acid (5.0 g, 30 mmol), MsOH (14.4 g, 150 mmol), and H_2O_2 (3.6 g of 88%, 93 mmol) afforded the product as yellow crystals (5.4 g, 93%) that were analyzed as 95.8% peracid by iodometric titration. Further purification was achieved by washing a CH_2Cl_2 solution (300 mL) of the crude product (5.3 g) with aqueous NaOH (0.038 M, 50 mL) then water (50 mL). Drying ($MgSO_4$) and solvent removal at room temperature afforded material of 98.8% purity: mp 139 °C (vigorous decomposition) (lit. 138 °C decomposition);[37] ν_{max}/cm^{-1} 3503 br, 3283 br, 1741 vs; δ_H ($CDCl_3$, 300 MHz) 8.20 (2H, dm, J = 9.0 Hz), 8.37 (2H, dm, J = 9.0 Hz), 11.56 (1H, s); δ_C ($CDCl_3$, 75 MHz) 123.7, 124.0, 130.6, 131.3, 166.1; *m*/*z* (ESI) found 182.0123, calcd for $C_7H_4NO_5$ $(M - H)^-$ 182.0089.

3-Methoxyperbenzoic acid.[44] Although Swern and co-workers[37] report that their procedure was unsuccessful in the synthesis of 3-methoxyperbenzoic acid, in our hands, slight changes to the method permitted its preparation. Stirred 3-methoxybenzoic acid (5.0 g, 33 mmol) in MsOH (14.7 g, 153 mmol) was cooled to 0 °C, and H_2O_2 (88%, 3.5 g, 91 mmol) was added dropwise at such a rate to keep the temperature below 50 °C. After 4 h, ice (50 g) was added, the mixture extracted with $CHCl_3$ (3 × 50 mL), and the combined organic extracts were washed with H_2O (50 mL) and dried ($MgSO_4$). Removal of solvent in vacuo at room temperature afforded a brown/yellow solid (3.7 g, 26% yield), 38% peracid by iodometric titration. A small quantity was purified for characterization by flash chromatography (R_f = 0.34, CH_2Cl_2 on silica), and upon cooling, the resulting colorless oil crystallized: mp 32−34 °C; ν_{max}/cm^{-1} 3516 br, 3265 br, 1732 vs, 925 w; δ_H ($CDCl_3$, 300 MHz) 3.85 (3H, s), 7.18 (1H, ddd, J = 8.3, 2.6, 1.0 Hz), 7.41 (1H, t, J = 7.9 Hz), 7.49 (1H, dd, J = 2.6, 1.8 Hz), 7.59 (1H, dt, J = 7.6, ∼1.2 Hz), 11.62 (1H, s); δ_C ($CDCl_3$, 75 MHz) 55.5, 113.6, 121.0, 121.6, 126.3, 130.0, 159.8, 168.0; *m*/*z* (ESI) found 167.0371, calcd for $C_8H_7O_4$ $(M - H)^-$ 167.0344.

4-Methoxyperbenzoic acid.[45] A solution of freshly prepared 4-methoxybenzoyl chloride (3.0 g, 18 mmol) in CH_2Cl_2 (6 mL) was added dropwise to a stirred suspension of aqueous H_2O_2 (93%, 3.0 g, 82 mmol) in CH_2Cl_2 (6 mL) at 0 °C. After 2.5 h at 0 °C, the mixture was poured into ice water (15 mL), extracted with CH_2Cl_2 (3 × 15 mL), and the combined extracts were washed with cold water (10 mL) and dried ($MgSO_4$). Rotary evaporation of solvent at room temperature yielded a white solid (3.1 g, yield 72%) that was analyzed as 68.2% peracid by iodometric titration. Further purification by flash chromatography (R_f = 0.3, cold CH_2Cl_2 on silica) achieved a purity of 84.1%: δ_H ($CDCl_3$, 500 MHz) 3.88 (3H, s), 6.97 (2H, d, J = 8.8 Hz), 7.95 (2H, d, J = 8.8 Hz), 11.62 (1H, br); δ_C ($CDCl_3$, 125 MHz) 55.5, 114.2, 121.9, 131.5, 164.4, 167.9; *m*/*z* (ESI) found 167.0368, calcd for $C_8H_7O_4$ $(M - H)^-$ 167.0344.

Electronic Structure Calculations. Geometry optimizations were carried out with the B3LYP method[46,47] using the 6-311++G-(d,p) basis set within the GAUSSIAN03 suite of programs.[48] All stationary points on the potential energy surface were characterized as either minima (no imaginary frequencies) or transition states (one imaginary frequency) by calculation of the frequencies using analytical gradient procedures. Frequency calculations provided zero-point energies, which were added to the calculated electronic energy. The minima connected by a given transition state were confirmed by inspection of the animated imaginary frequency using the MOLDEN package[49] and by intrinsic reaction coordinate calculation.[50,51]

Acknowledgment. S.J.B. acknowledges the financial support of the University of Wollongong (URC New Researcher Grant), the Institute for Biomolecular Science, and the Australian Research Council (DP0452849). We also acknowledge the support of the Australian Partnership for Advanced Computing (ANU, Canberra) for a generous allocation of supercomputing time.

Supporting Information Available: Electronic energies, zero-point energies, and molecular geometries (as Cartesian coordinates) for all stationary points discussed in the text. This material is available free of charge via the Internet at http://pubs.acs.org.

JO060730A

(43) Pande, C. S.; Jain, N. *Synth. Commun.* **1988**, *18*, 2123.
(44) Blake, R. C., II; Coon, M. J. *J. Biol. Chem.* **1980**, *255*, 4100.
(45) Konen, D. A.; Silbert, L. S. *J. Org. Chem.* **1971**, *36*, 2162.
(46) Becke, A. D. *J. Chem. Phys.* **1993**, *98*, 1372.
(47) Lee, C. T.; Yang, W. T.; Parr, R. G. *Phys. Rev. B: Condens. Matter* **1988**, *37*, 785.
(48) Frisch, M. J.; Trucks, G. W.; Schlegel, H. B.; Scuseria, G. E.; Robb, M. A.; Cheeseman, J. R.; Montgomery, J. A., Jr.; Vreven, T.; Kudin, K. N.; Burant, J. C.; Millam, J. M.; Iyengar, S. S.; Tomasi, J.; Barone, V.; Mennucci, B.; Cossi, M.; Scalmani, G.; Rega, N.; Petersson, G. A.; Nakatsuji, H.; Hada, M.; Ehara, M.; Toyota, K.; Fukuda, R.; Hasegawa, J.; Ishida, M.; Nakajima, T.; Honda, Y.; Kitao, O.; Nakai, H.; Klene, M.; Li, X.; Knox, J. E.; Hratchian, H. P.; Cross, J. B.; Bakken, V.; Adamo, C.; Jaramillo, J.; Gomperts, R.; Stratmann, R. E.; Yazyev, O.; Austin, A. J.; Cammi, R.; Pomelli, C.; Ochterski, J. W.; Ayala, P. Y.; Morokuma, K.; Voth, G. A.; Salvador, P.; Dannenberg, J. J.; Zakrzewski, V. G.; Dapprich, S.; Daniels, A. D.; Strain, M. C.; Farkas, O.; Malick, D. K.; Rabuck, A. D.; Raghavachari, K.; Foresman, J. B.; Ortiz, J. V.; Cui, Q.; Baboul, A. G.; Clifford, S.; Cioslowski, J.; Stefanov, B. B.; Liu, G.; Liashenko, A.; Piskorz, P.; Komaromi, I.; Martin, R. L.; Fox, D. J.; Keith, T.; Al-Laham, M. A.; Peng, C. Y.; Nanayakkara, A.; Challacombe, M.; Gill, P. M. W.; Johnson, B.; Chen, W.; Wong, M. W.; Gonzalez, C.; Pople, J. A. *Gaussian 03*, revision C.02; Gaussian Inc.: Wallingford, CT, 2004.
(49) Schaftenaar, G.; Noordik, J. H. *J. Comput.-Aided Mol. Des.* **2000**, *14*, 123.
(50) Gonzalez, C.; Schlegel, H. B. *J. Chem. Phys.* **1989**, *90*, 2154.
(51) Gonzalez, C.; Schlegel, H. B. *J. Phys. Chem.* **1990**, *94*, 5523.